J. Fluid Mech. (1994), *vol.* 281, *pp.* 33–50

The effects of thermal conditions on the cell sizes of two-dimensional convection

By MASAKI ISHIWATARI, SHIN-ICHI TAKEHIRO AND YOSHI-YUKI HAYASHI

Department of Earth and Planetary Physics, Faculty of Science, University of Tokyo, Bunkyo, Tokyo, 113, Japan

(Received 8 October 1993 and in revised form 28 June 1994)

The effects of thermal conditions on the patterns of two-dimensional Boussinesq convection are studied by numerical integration. The adopted thermal conditions are (i) the heat fluxes through both upper and lower boundaries are fixed, (ii) the same as (i) but with internal cooling, (iii) the temperature on the lower boundary and the heat flux through the upper boundary are fixed, (iv) the same as (iii) but with internal cooling, and (v) the temperatures on both upper and lower boundaries are fixed. The numerical integrations are performed with $Ra = 10^4$ and $Pr = 1$ over the region whose horizontal and vertical lengths are 8 and 1, respectively.

The results confirm that convective cells with the larger horizontal sizes tend to form under the conditions where the temperature is not fixed on any boundaries. Regardless of the existence of internal cooling, one pair of cells spreading all over the region forms in the equilibrium states. On the other hand, three pairs of cells form and remain when the temperature on at least one boundary is fixed. The formation of single pairs of cells appearing under the fixed heat flux conditions shows different features with and without internal cooling. The difference emerges as the appearance of a phase change, whose existence can be suggested by the weak nonlinear equation derived by Chapman & Proctor (1980).

1. Introduction

It is well known that in Bénard convection, which occurs between two horizontal isothermal boundaries, the horizontal and the vertical scales of the convective cells are of the same order for moderate values of the Rayleigh number (e.g. Rayleigh 1916; Schlüter, Lortz & Busse 1965; Busse & Whitehead 1971; Ogura 1971), although the cells with large horizontal scales can be formed at higher Rayleigh number (Rothermel & Agee 1986).† On the other hand, when the heat fluxes through both upper and lower boundaries are fixed, the horizontal scale of the equilibrium convective cells are reported to be much larger than the vertical scale even when the moderated values of the Rayleigh number are adopted (e.g. Sparrow, Goldstein & Jonsson 1964; Hurle, Jakeman & Pike 1967; Jakeman 1968; Sasaki 1970; Hewitt, McKenzie & Weiss 1980; Chapman & Proctor 1980; Chapman, Childress & Proctor 1980). However, as

† The horizontal scales of Bénard convective cells for high Rayleigh number seem to be controversial. For example, at the value of Rayleigh number 600 times larger than the critical value, Rothermel & Agee (1986) present cells with a horizontal scale about ten times larger than the layer depth in their two-dimensional calculations. However, Sykes & Henn (1988) do not obtain such large cells in a similar situation but with a different numerical scheme.

described below, there are several inconsistencies between the numerical results and the weak nonlinear descriptions of fixed flux convection presented so far.

Within the framework of linear theory, Sparrow *et al.* (1964) show that the critical wavelength for the fixed flux condition is infinite. This peculiar characteristic is used by Hurle *et al.* (1967) and Jakeman (1968) for the description of crystallization in metallic liquids and Sasaki (1970) for the description of mesoscale cellular convection observed behind midlatitude cyclones in the atmosphere. However, the critical wavelength cannot be regarded as a very good measure of the cell sizes at Rayleigh numbers larger than the critical value. Since the maximum growth rate curve approaches the short-wavelength region immediately as the Rayleigh number increases above the critical value (see Appendix A), the linear stability theory predicts that the aspect ratio, which is defined as the ratio of the horizontal scale to the vertical scale of convective cells, should be of the order of unity at least at the onset of convection.

Two-dimensional nonlinear calculations for the fixed flux conditions are performed by Hewitt *et al.* (1980, hereinafter referred to as HMW80). The experiments are carried out in the rectangular region of $0 \leqslant x \leqslant 8$ and $0 \leqslant z \leqslant 1$ with the Rayleigh number $Ra = 2.4 \times 10^3 \sim 1.4 \times 10^6$ and the Prandtl number $Pr = \infty$ (the definitions of Ra and Pr are given in §2). This values of the Prandtl number is adopted because they are considering mantle convection. The results of HMW80 show that, when $Ra \geqslant 2.4 \times 10^5$, the horizontal scale of convective cells grows gradually until the whole computational domain is covered by a single convective cell.

The theoretical description of the horizontal growth of convective cells is made by Chapman & Proctor (1980, hereinafter referred to as CP80). CP80 derives a weak nonlinear equation governing the leading-order evolution of temperature at $Ra \simeq Ra_c$, which exemplifies that an equilibrium solution is unstable to a disturbance of the longer wavelengths. HMW80 points out that their numerical results obtained at $Ra \geqslant 2.4 \times 10^5$ are compatible with the theory of CP80. However, we have to note here that, a single convective cell spreading all over the computational domain is not observed in the results of HMW80 with the smaller values of the Rayleigh number where the amplitude expansion of CP80 is expected to be more reliable.

Two-dimensional convection driven by an internal homogeneous heat source instead of the heat flux through the lower boundary is also considered by HMW80. The calculations are performed with the same parameters as the fixed heat flux experiments. The results show that, for all cases, a single convective cell spreading all over the domain does not appear, but three to four cells with unequal sizes remain. The corresponding weak nonlinear theory is developed by Chapman *et al.* (1980, hereinafter referred to as CCP80), which predicts that an equilibrium state with multiple cells in a given horizontal domain is unstable and finally a single cell should appear. For the case of convection driven by the internal heat source, the results of nonlinear calculation are not compatible with the expectation of the weak nonlinear theory.

In this study we once again perform numerical calculations of two-dimensional Boussinesq convection under various thermal conditions. We reconsider the correspondence between the numerical results and the weak nonlinear theory. Focus is placed on the cases where the heat flux is fixed at the boundaries in order to exemplify when and how the convective cells grow horizontally. The calculations under fixed temperature conditions are also performed for the purpose of comparing flow patterns to those of the fixed flux cases. We have to note here that, throughout this paper, we assume $Pr = 1$ rather than $Pr = \infty$ of HMW80. Moreover, when the convection is driven internally, it is assumed to be by internal cooling rather than internal heating. This configuration models the atmospheres which are heated at the surface and cooled

internally by radiation. The reason why we adopt those conditions is that an investigation of the appearance of convective cells with large aspect ratios can be useful in describing the atmospheric phenomena. For example, 30–60 day oscillation observed in the equatorial atmosphere has the zonal wavenumber one structure (Madden & Julian 1972; Numaguti & Hayashi 1991*a*, *b*). It is usually accepted that the large aspect ratio of 30–60 day oscillation can be interpreted as the characteristic of moist convection (Xie 1994). However, the embedded dynamical structure is still unclear and hence it is of interest to learn dry convection also gives a large aspect ratio in certain cases.

In §2 we will summarize the mathematical formulation and the numerical method utilized. In §3 the results of numerical integrations are presented. It is shown that the fixed flux conditions both with and without internal cooling give a single pair of convective cells, although the evolution of the cells are different. In §4, we try to describe the difference of the growth of cells by the use of the weak nonlinear theory of CP80. It is suggested that the growth of disturbances for the internal cooling case depends on the phase relation between the equilibrium solution and the unstable disturbances.

2. Model

We consider two-dimensional Boussinesq fluid in a laterally periodic domain. The thermal conditions adopted here are illustrated in figure 1. In case FF (figure 1*a*), the heat fluxes through the upper and lower boundaries are fixed to be constant and equal to each other. In case FQ (figure 1*b*), the heat supplied by the constant heat flux through the lower boundary is equal to that lost by the internal homogeneous cooling. The heat flux through the upper boundary is zero. This case corresponds to the reverse of the HMW80 model of mantle convection which is driven by the internal heat source. In case TF (figure 1*c*), the temperature on the lower boundary and the heat flux through the upper boundary are fixed. In case TQ (figure 1*d*), the temperature on the lower boundary is fixed and the homogeneous internal cooling exists. The heat flux through the upper boundary is zero as it is in case FQ. In case TT (figure 1*e*), the temperatures on both lower and upper boundaries are fixed. This corresponds to the usual Bénard convection model.

The physical quantities of the Boussinesq fluid are non-dimensionalized in the following way. The horizontal and vertical coordinates x, z are non-dimensionalized by the fluid depth d, time t is by d^2/κ, velocity (u, w) is by κ/d, where κ is the thermal diffusivity. Temperature T is non-dimensionalized by $F_0 d/\kappa$ in cases FF, FQ, TF and TQ, where F_0 is the heat flux fixed or averaged on the boundary. In case TT, it is non-dimensionalized by the temperature difference between upper and lower boundary ΔT.

According to the scales described above, the Rayleigh number Ra is defined as follows. In cases FF, case FQ, case TF and case TQ,

$$Ra \equiv \frac{\tilde{\alpha} g F_0 d^4}{\nu \kappa^2}. \tag{1}$$

and in case TT,

$$Ra \equiv \frac{\tilde{\alpha} g \Delta T d^3}{\nu \kappa}. \tag{2}$$

Here $\tilde{\alpha}$ is the coefficient of volume expansion, ν is the kinematic viscosity, g is the acceleration due to gravity.

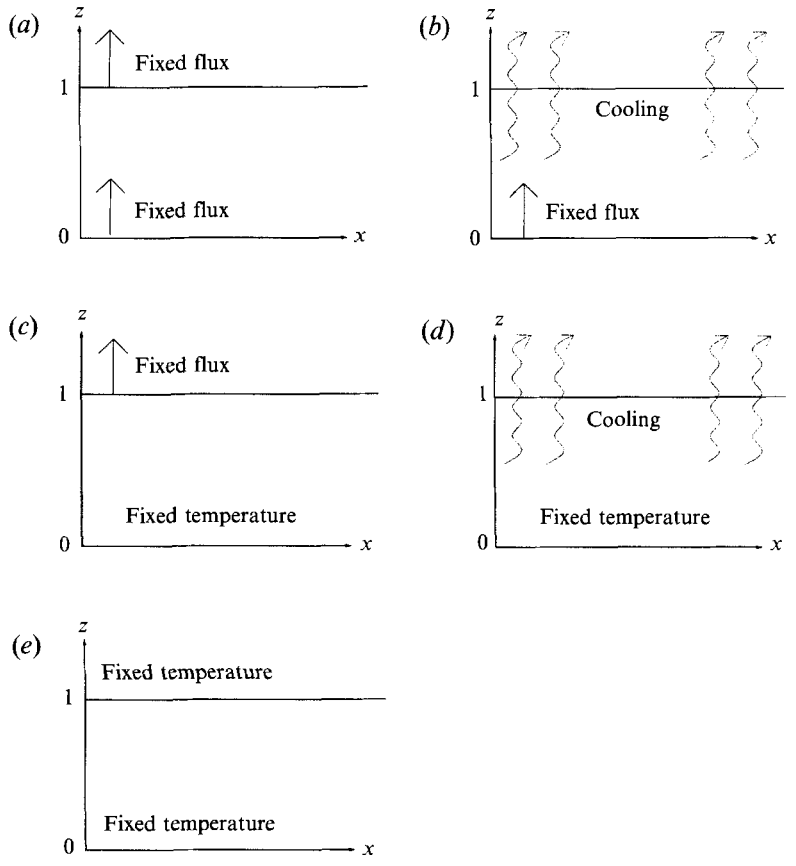

FIGURE 1. Illustration of the thermal conditions for numerical experiments. (*a*) Case FF, (*b*) case FQ, (*c*) case TF, (*d*) case TQ, (*e*) case TT.

The non-dimensionalized equations are given by

$$\frac{\partial}{\partial t}\nabla^2\psi+\left(\frac{\partial\psi}{\partial z}\frac{\partial}{\partial x}-\frac{\partial\psi}{\partial x}\frac{\partial}{\partial z}\right)\nabla^2\psi = Pr\,\nabla^2\nabla^2\psi - Pr\,Ra\frac{\partial T}{\partial x}, \tag{3}$$

$$\frac{\partial T}{\partial t}+\left(\frac{\partial\psi}{\partial z}\frac{\partial T}{\partial x}-\frac{\partial\psi}{\partial x}\frac{\partial T}{\partial z}\right) = \nabla^2 T+Q, \tag{4}$$

where ψ is the stream function, $Pr \equiv \nu/\kappa$ is the Prandtl number. The non-dimensionalized heating rate Q and the thermal conditions are summarized in table 1. The adopted kinematic and stress conditions are the same for all cases:

$$\psi = \frac{\partial^2\psi}{\partial z^2} = 0 \quad (\text{at } z = 0, 1). \tag{5}$$

All calculations are performed with $Pr = 1$ and $Ra = 10^4$. The calculation domain is restricted to the rectangular region of $0 \leqslant x \leqslant 8$ and $0 \leqslant z \leqslant 1$. The numbers of grid points in the horizontal and vertical directions are 256 and 32, respectively. Under the resolution adopted here, the thermal boundary layer near the temperature fixed boundaries can be resolved. Those values are determined referring to those of

	Upper boundary	Lower boundary	Heating rate
Case FF	$\frac{dT}{dz} = -1$	$\frac{dT}{dz} = -1$	$Q = 0$
Case FQ	$\frac{dT}{dz} = 0$	$\frac{dT}{dz} = -1$	$Q = -1$
Case TF	$\frac{dT}{dz} = -1$	$T = 1$	$Q = 0$
Case TQ	$\frac{dT}{dz} = 0$	$T = 1$	$Q = -1$
Case TT	$T = 0$	$T = 1$	$Q = 0$

TABLE 1. The list of thermal conditions adopted in the numerical experiments

HMW80. Note that our lateral boundary conditions are periodic, while those of HMW80 are insulated walls.

The system is integrated by a finite-difference method. Advection terms are expressed in terms of the Arakawa Jacobian. Time integrations are performed by the leapfrog scheme with the diffusion terms being lagging by one timestep to avoid computational instability. To remove the computational modes, the Heun scheme is used at every twenty timesteps. Timestep of integrations is 10^{-4} for all cases. The initial conditions are the conductive solutions added by a point temperature perturbation with the value of 10^{-2} placed at $(x, z) = 4, \frac{1}{32})$.

3. The results of numerical integrations

3.1. *The fixed heat flux case (case FF)*

Figure 2 shows the vorticity and temperature fields obtained in case FF. At the onset of convection, cells with wavenumber $k \simeq 4 \times 2\pi/8$ appear (figure 2*a*). This wavenumber is slightly smaller than $k = 3.9$ which is the wavenumber of the most unstable mode given by the linear theory (Appendix A). After a pair of cells at $x = 8$ diminish at $t = 1.15$, cells at $x = 2$ and $x = 6$ shrink and disappear at $t = 7.85$ (figure 2*b*, *c*). This distinction of cells appears in the flow field as a conjunction of the upward and downward flows, while in the temperature field as a conjunction of the warm and cold regions. In the final steady state, there appears one pair of cells spreading all over the region (figure 2*d*).

The change of dominant wavenumber can be clearly observed in figure 3 which shows the time evolution of the amplitude of the Fourier components determined by

$$T(x, z) = \frac{1}{128} \sum_{n=0}^{128} A_n(z) \cos\left(\frac{2\pi n}{L} x + \theta_n\right), \tag{6}$$

where $L = 8$ is the horizontal length of the domain. Figure 3 shows the values of A_n for $z = \frac{1}{4}$ and $n = 0, 1, 2, 3, 4$. At $t = 1.15$, the amplitude of $n = 3$ component becomes dominant. However, the amplitude of $n = 1$ component grows steadily at a growth rate of about 0.17 until $t \sim 7.8$, and finally increases abruptly. The growth rate of 0.17 is

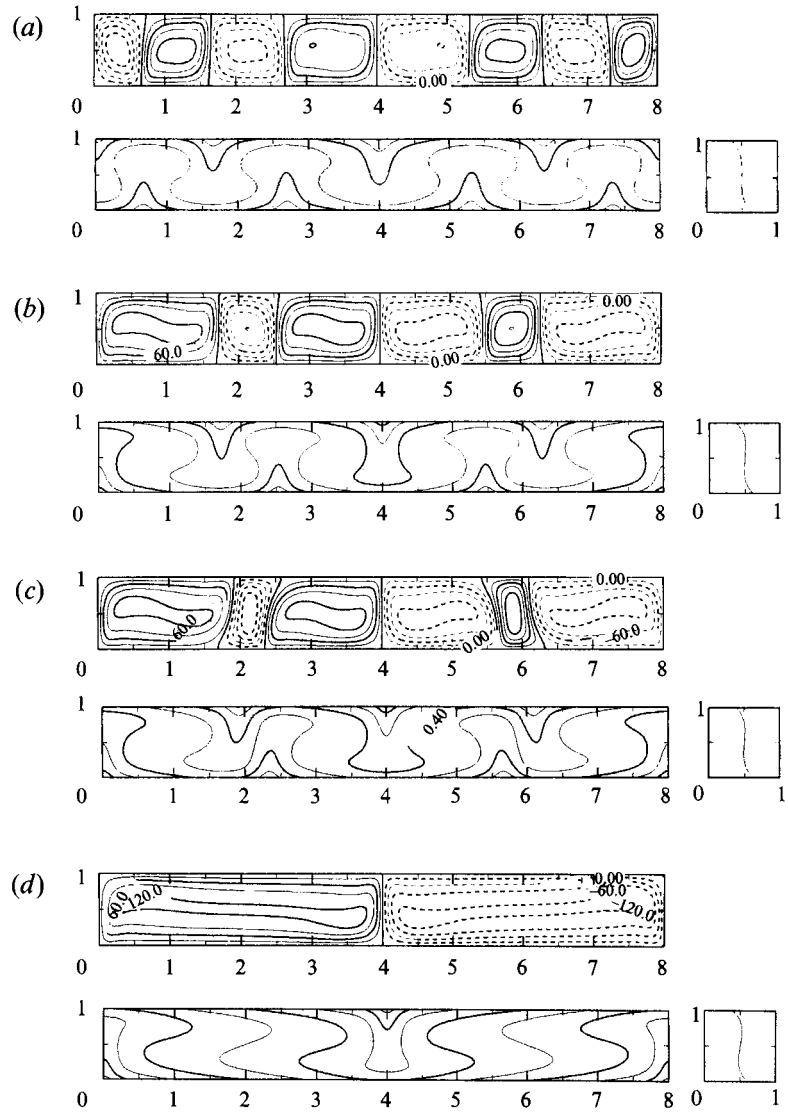

FIGURE 2. The vorticity fields (upper figures) and the temperature fields (lower figures) of case FF at (*a*) $t = 0.5$, (*b*) $t = 7$, (*c*) $t = 7.7$, and (*d*) $t = 15$. The charts on the right-hand side are the horizontal average of the temperature. The contour intervals of vorticities and temperatures are 30 and 0.1, respectively.

quite smaller than the linear growth rate of the most unstable mode which is about 40. The phase of each Fourier component θ_n does not change in due course (not shown).

We perform several integrations with various spatial resolutions. The obtained result using the finer grid of 512×64 resembles figure 2. One pair of cells appear at $t = 8.2$ in the 512×64 case and the difference of the amplitudes of stream function in the steady states is 1.6%. The experiments using coarser grids of 128×16 and 64×8 also yield the result that cells with wavenumber one form in the steady states.

The elongation of convective cells under the fixed heat flux condition is also obtained by HMW80 with $Pr = \infty$ and $Ra = 2.4 \times 10^5$, 1.4×10^6. However, at the parameters $Ra = 2.4 \times 10^3$, 2.4×10^4, HMW80 does not yield a single cell spreading all over the

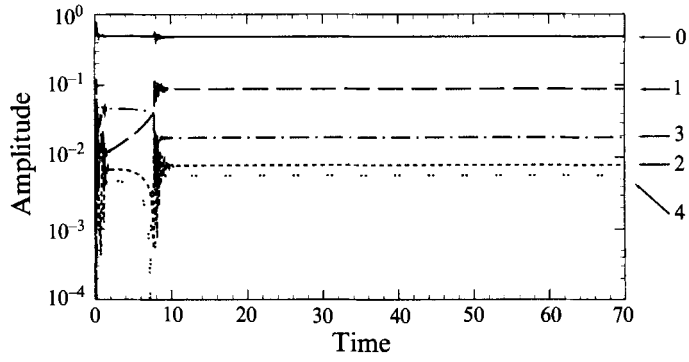

FIGURE 3. The time evolution of amplitudes of Fourier components of temperature at $z = \frac{1}{4}$ in case FF. The numbers indicate the wavenumber of each component.

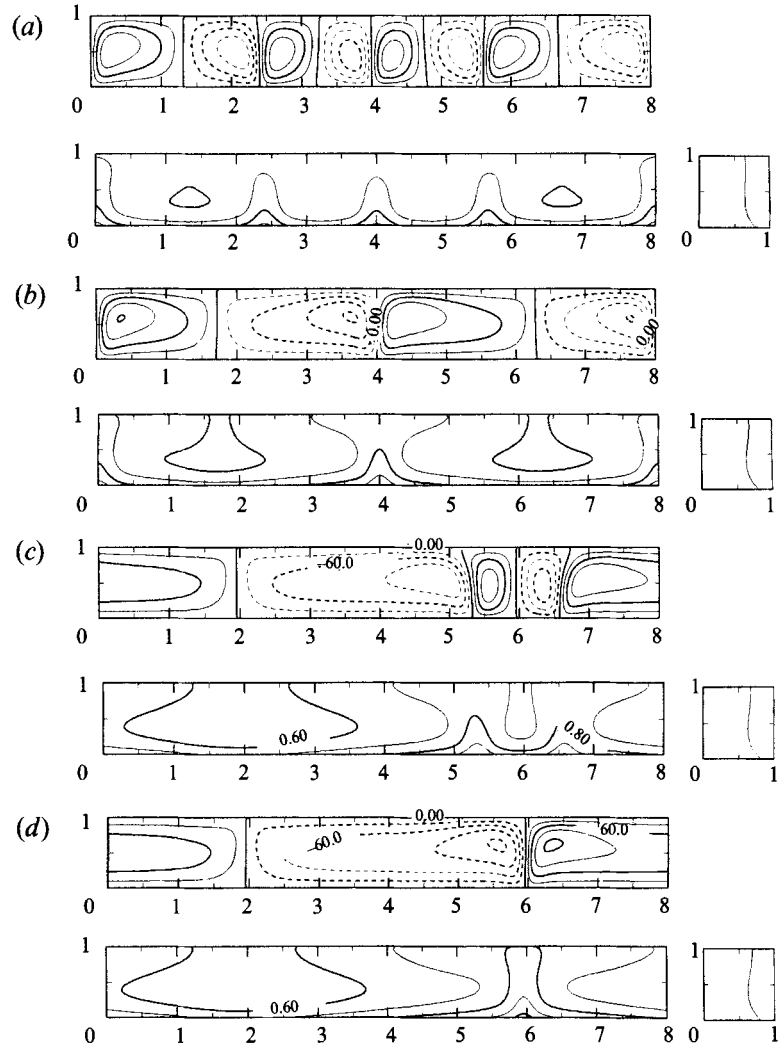

FIGURE 4. Same as figure 2 but for case FQ at (*a*) $t = 1$, (*b*) $t = 7$, (*c*) $t = 54$, and (*d*) $t = 70$.

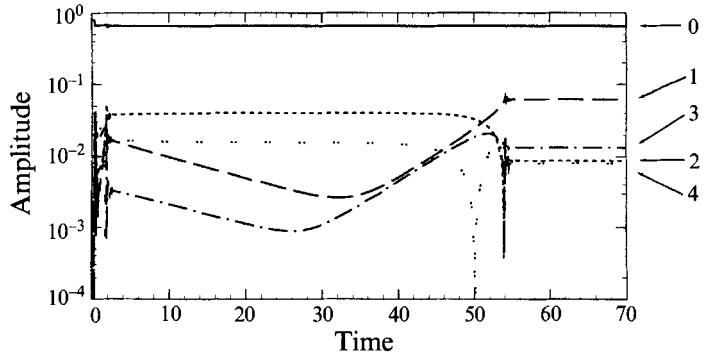

FIGURE 5. Same as figure 3 but for case FQ.

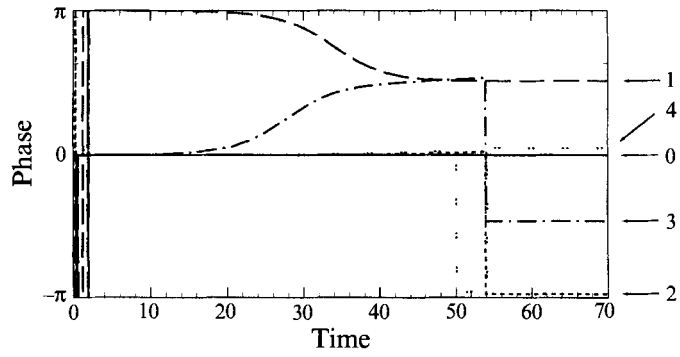

FIGURE 6. Same as figure 5 but for the phases of Fourier components.

region. This contrasts to our result shown in figures 2 and 3 calculated at $Ra = 10^4$, although the value of the Prandtl number is different from that of HMW80. A discussion on this point will be given in §5.

3.2. *The fixed heat flux case with internal cooling (case FQ)*

The time evolution of the vorticity and temperature fields of case FQ is shown in figure 4. As in case FF, the wavenumber of convective cells observed at the onset of convection is $k \simeq 4 \times 2\pi/8$, as is expected by the linear theory (Appendix A). In the final steady state, there appears one pair of cells spreading all over the region. However, the evolution process of the cells differs from that of case FF. Cells with wavenumber two instead of three form in the intermediate state (figure 4*b*). Then, after a very long time, there appear cells with wavenumber one. The change of dominant wavenumber appears in the flow field as a distinction of the negative and positive vorticities and in the temperature field as a connection of two warm regions. It is worth noting that a phase change occurs in due course. The position of upward flow in the final steady state is at $x = 6$ as shown in figure 4(*d*), while those of the previous state are at $x = 0$ and $x = 4$. The phase of the steady state is shifted by $\frac{1}{2}\pi$ compared to that at $t = 7$.

The change of dominant wavenumber accompanied by the phase shift is clearly shown in the behaviour of the Fourier components as illustrated in figures 5 and 6. The amplitude of wavenumber one component decreases at first and then increases from $t \sim 32$ with the growth rate of about 0.17. This curious behaviour corresponds to the phase evolution of the wavenumber one component shown in figure 6. In other words,

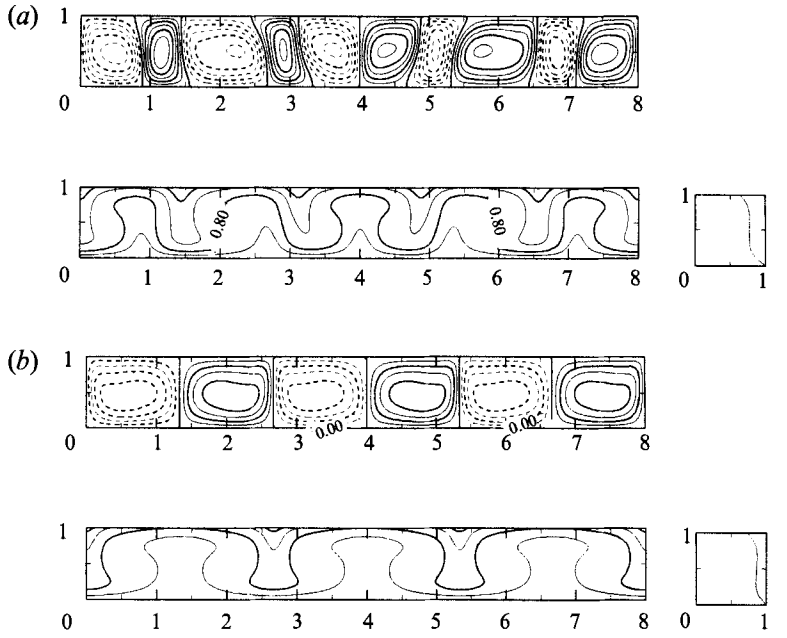

FIGURE 7. Same as figure 2 but for case TF at (*a*) $t = 0.5$, (*b*) $t = 10$.

the decay of the sine component whose symmetry is the same as that of the initial perturbation appears in the first change of the amplitude (figure 5), while the growth of the cosine component whose initial amplitude is at the noise level appears in the latter change of the amplitude.

The long period it takes for a single pair of cells to emerge in case FQ is due to the fact that the growing cosine component starts from the numerical noise level. The growth rate of the wavenumber one component in case FF is almost the same as that of the growing phase of case FQ. In case FF, a single pair of cells emerges promptly because the initial disturbance and the growing component has the same symmetry.

The initial condition dependency of the formation of a single pair of cells is tested by performing a calculation starting from a random disturbance instead of a point disturbance. A random white noise with the mean magnitude of 0.01 is utilized as an initial value for temperature. The result confirms that the wavenumber one component becomes dominant in the final steady state (not shown).

The result that cells with wavenumber one appear in case FQ is consistent with the expectation given by the weak nonlinear calculation of CCP80. However, the existence of the phase change has not been discussed in CCP80. We will return to this problem in §4. The full nonlinear calculations corresponding to case FQ performed by HMW80 with $Pr = \infty$ do not yield cells spreading all over the region. The discrepancy between the results of HMW80 and ours will be discussed in §5.

We finally note that the equilibrium state of case FQ (figure 4*d*) is slightly different from that of case FF. In case FF the upward and downward regions are symmetric (figure 2*d*), while in case FQ an asymmetric structure with a narrow upward region and a wide downward region appears. According to figure 4(*d*), the width of the upward region is about 1.78, while that of the downward region is 6.22. HMW80 also gives the similar asymmetric structure in the results corresponding to case FQ. The existence of asymmetry between upward and downward regions is often considered as a

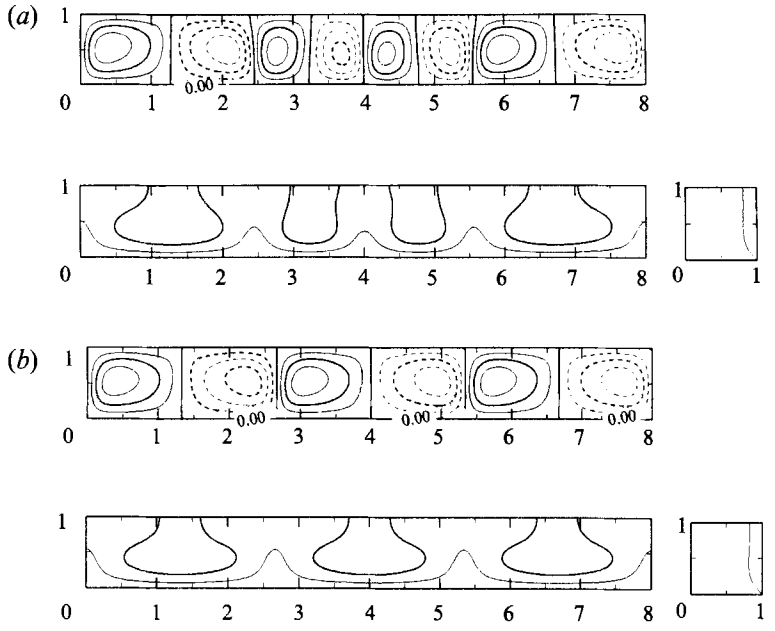

FIGURE 8. Same as figure 2 but for case TQ at (*a*) $t = 1$, (*b*) $t = 10$.

characteristic of atmospheric moist convection (Bjerknes 1938). However, it may be worth noting that such asymmetry does exist in dry convection driven by internal cooling.

3.3. *The fixed temperature cases (cases TF, TQ, TT)*

The result of case TF is shown in figure 7. At the onset of convection, there appear cells with wavenumber five, as is expected from the linear theory (Appendix A). At $t = 0.8$, a cell with positive vorticity at $x = 3$ and a cell with negative vorticity at $x = 5$ diminish. However, unlike the evolutions in cases FF and FQ, the change of cell size does not occur after the formation of cells with wavenumber three, according to our calculation continued up to $t = 70$. Figure 8 shows the result of case TQ. Likewise case TF, does not form one pair of cells spreading all over the region. At the onset of convection, cells with wavenumber four appear (figure 8*a*). At $t = 1.7$ cells with positive and negative vorticities diminish at $x = 4$ and cells with wavenumber three form, and then the system reaches its steady state, at least up to the end of our calculation at $t = 70$. As in case FQ, the asymmetric structure of a narrow upward region and a wide downward region emerges. The widths of upward and downward regions are 1.22 and 1.56, respectively. Calculations corresponding to cases TF and TQ are performed by HMW80 with $Ra = 2.4 \times 10^5$ and $Pr = \infty$. The results also show that no cell grows to spread all over the region.

We perform the calculation of case TT for the purpose of comparison with the cases presented so far. The result is shown in figure 9. At the onset of convection, there appear cells with wavenumber five (figure 9*a*). At $t = 3.1$, cells with positive and negative vorticity diminish at $x = 4$, and at $t = 4.55$ cells at $x = 8$ disappear. The calculation is performed up to $t = 70$, but no change is observed. The final steady cells are composed of wavenumber three. We may say that the condition that the temperature on at least one boundary is fixed is the dominant factor on the scale selection of convective cells. Note that the average heat flux through the lower boundary of case TT differs from that of case TF and case TQ.

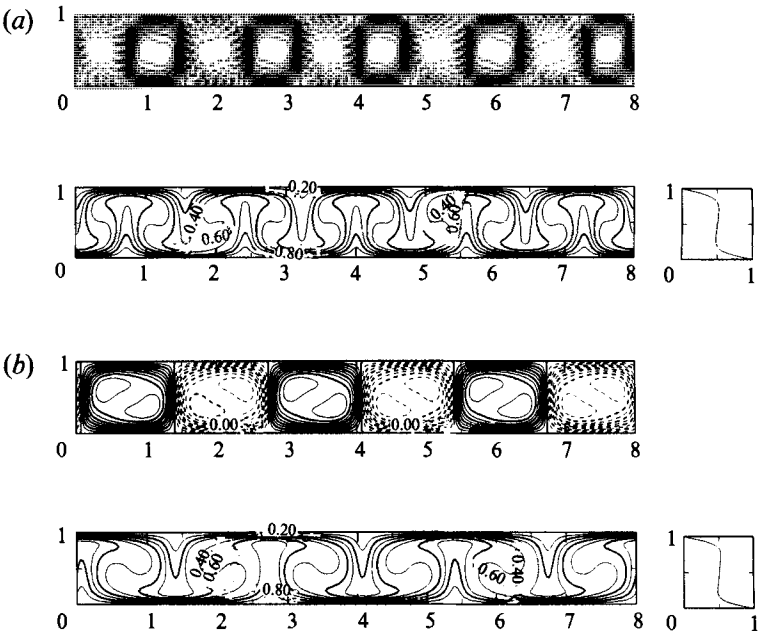

FIGURE 9. Same as figure 2 but for case TT at (*a*) $t = 0.5$, (*b*) $t = 10$.

4. Description of phase change by weak nonlinear theory

The weak nonlinear theory which explains the formation of horizontally elongated cells obtained in cases FF and FQ is considered by CP80 and CCP80. In this section, we try to describe the phase change appearing in case FQ by the use of the equation derived by CP80. As described below, the form of the governing equation does not change even when $Pr = \infty$, the following discussion can be applied to the situation which includes the cases considered by HMW80. Unfortunately, we must confess beforehand that the discussion below breaks down at the value of the Rayleigh number with which the numerical integrations in §3 are performed. However, since the qualitative behaviour of the solutions resembles the numerical results presented in §3, we keep the following argument in order to suggest the dynamical structure embedded in the numerical results.

The derivation of the equation governing the leading-order evolution of temperature follows the argument of CP80 (Appendix B). We assume $Ra = Ra_c + \mu^2\epsilon^2$ ($\epsilon \ll 1$, $\mu = O(1)$) and rescale time and horizontal length as $\epsilon^4 t \to t, \epsilon x \to x$. Then, temperature and stream function are expanded in powers of ϵ as follows:

$$T = \theta_0 + \epsilon^2\theta_2 + \ldots, \tag{7}$$

$$\psi = \epsilon\phi_0 + \epsilon^3\phi_2 + \ldots . \tag{8}$$

We solve the $O(\epsilon^0)$ equations and can show that θ_0 is independent of z. The $O(\epsilon^2)$ and $O(\epsilon^4)$ equations give the time evolution of $\theta_0(x, t)$:

$$\frac{\partial\theta_0}{\partial t} = -\mu^2\frac{\partial^2\theta_0}{\partial x^2} - \frac{\partial^4\theta_0}{\partial x^4} + \frac{\partial}{\partial x}\left\{\left(\frac{\partial\theta_0}{\partial x}\right)^3\right\} - \alpha\frac{\partial}{\partial x}\left(\frac{\partial\theta_0}{\partial x}\frac{\partial^2\theta_0}{\partial x^2}\right). \tag{9}$$

Here, we have rescaled the variables so as to simplify the equation. Note that $\alpha \equiv 0$ in case FF. For case FQ, $\alpha = -0.3$ with the parameters used in our experiments. The dependency of the Prandtl number appears only in α.

In the case of $\alpha = 0$, CP80 analytically finds the steady solutions of (9) and investigates their stability. In the case of $\alpha \neq 0$, CP80 and CCP80 numerically obtain steady solutions and investigate their stability. From these calculations, CP80 and CCP80 conclude that a steady solution is unstable to a perturbation of the longer wavelength regardless of the existence of heat source.

In order to discuss the phase change observed in case FQ, a simpler analysis than those of CP80 and CCP80 can be made by utilizing a highly truncated system of the Fourier series. Let us assume that the system consists only of wavenumber m and one. The steady solution is given by the cells with wavenumber m. We will analyse its stability to the perturbation with wavenumber one.

θ_0 of this truncated system is written by

$$\theta_0 = \tfrac{1}{2}(S(t)\,\mathrm{e}^{\mathrm{i}px} + S^*(t)\,\mathrm{e}^{-\mathrm{i}px}) + \tfrac{1}{2}(M(t)\,\mathrm{e}^{mipx} + M^*(t)\,\mathrm{e}^{-mipx}), \tag{10}$$

where $p = 2\pi/L$ and * represents complex conjugate. Substituting above expression into (9), we obtain

$$\frac{\partial S}{\partial t} = (\mu^2 - p^2)p^2 S - \tfrac{3}{4}p^4\{(|S|^2 + 2m^2|M|^2)S + \delta_{m3}m(2-m)S^{*2}M\} + \delta_{m2}\frac{\alpha p^4}{2}m(m-1)^2 S^* M, \tag{11}$$

$$\frac{\partial M}{\partial t} = m^2(\mu^2 - m^2p^2)p^2 M - \tfrac{3}{4}p^4\{(m^4|S|^2 + 2m^2|M|^2)M - \delta_{m3}S^3\} - \delta_{m2}\alpha p^4 S^2, \tag{12}$$

where δ_{ij} is Kronecker's delta. The steady solution of wavenumber m can be given by

$$M_B^{(m)} = \left(\frac{4(\mu^2 - m^2p^2)}{3m^2p^3}\right)^{1/2}. \tag{13}$$

Here, the phase of the steady state is set to be zero for simplicity. We must have $\mu^2 - m^2p^2 > 0$ in order for a steady state to exist. The perturbation equations are obtained by placing $S = S'$, $M = M_B^{(m)} + M'$ and substituting them into (11) and (12),

$$\frac{\partial S'}{\partial t} = \{(2m^2-1)p^2 - \mu^2\}p^2 S' + \delta_{m2}\alpha p^3(m-1)^2\left(\frac{\mu^2 - m^2p^2}{3}\right)^{1/2} S'^*, \tag{14}$$

$$\frac{\partial M'}{\partial t} = -m^2p^2(\mu^2 - m^2p^2)(M' + M'^*). \tag{15}$$

The growth rates of the perturbation S' are

$$\sigma_\pm = \{(2m^2-1)p^2 - \mu^2\}p^2 \pm \delta_{m2}\alpha p^3(m-1)^2\left(\frac{\mu^2 - m^2p^2}{3}\right)^{1/2}, \tag{16}$$

which means that the wavenumber one component can grow provided that μ is sufficiently small. The growth rates of M' are 0 and $-2m^2(\mu^2 - m^2p^2)p^2 < 0$. Since the latter is always negative, the steady solution is stable to a perturbation of wavenumber m.

In the case of $m = 2$ and when the internal cooling exists, namely $\alpha < 0$, σ_- is greater than σ_+. The eigenfunction corresponding to the larger eigenvalue σ_- is

$$S' = -i. \tag{17}$$

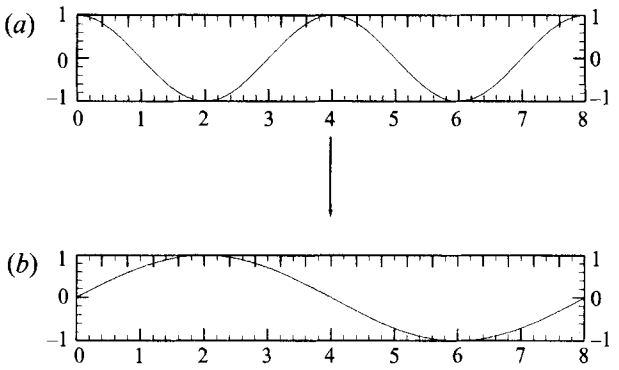

FIGURE 10. A typical configuration of (*a*) the wavenumber two basic state and (*b*) the most unstable wavenumber one disturbance.

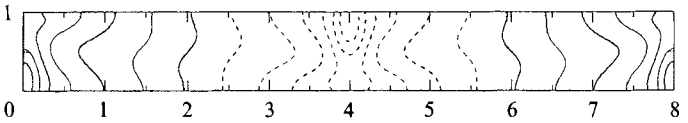

FIGURE 11. The temperature deviation $T-\bar{T}$ of case FF. The contour interval is 0.05. The maximum and minimum values of contour levels are 0.30 and -0.30 respectively.

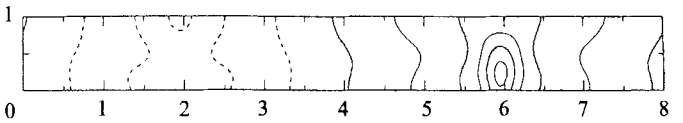

FIGURE 12. Same as figure 12 but for case FQ. The maximum and minimum values of contour levels are 0.25 and -0.15, respectively.

Therefore, the largest growth rate is acquired by the perturbations $\pm\cos(px+\frac{3}{2}\pi)$, which are out of phase with the basic steady state $\cos(2px)$. The relationship between the basic steady state and the most unstable disturbance is illustrated in figure 10. If we describe the behaviour in terms of the positions of downward and upward regions, since the negative value of θ_0 corresponds to a downward region, the position of one of the downward regions is prohibited to move. If internal cooling does not exist, namely $\alpha = 0$, the growth rate of disturbance is independent of its phase.

In case FQ, cells with wavenumber one emerge from the cells with wavenumber two. During the elongation of the cells, the downward region at $x = 2$ does not move (figure 4). This result is consistent with the discussion above. Although the asymmetry between the upward and the downward region is remarked in §3.2, such an asymmetry does not appear in the truncated system used here and is independent of the existence of the phase shift.

The simple discussion presented above is valid only when $Ra \sim Ra_c$. Actually, $\sigma_\pm$ is negative at the value of the Rayleigh number used in our numerical integrations. It is interesting, however, that the behaviour at $Ra \sim Ra_c$ still agrees with the numerical solutions. The temperature deviation from the horizontal mean, $T-\bar{T}$, of cases FF and FQ are shown in figures 11 and 12, which may be considered to be independent of z. It seems that the dynamical structure at $Ra \sim Ra_c$ is maintained even at $Ra = 10^4$.

5. Discussion

In this section, we will discuss the difference between our results and those of HMW80. According to the results of HMW80, cells with wavenumber one are not expected to emerge at $Ra = 10^4$. The discrepancy can be attributed to the difference of integration time. In our case FF, it takes 7 dimensionless time units for the cells to spread all over the region. On the other hand, in the case at $Ra = 2.4 \times 10^4$ of HMW80, the integration is continued only up to 1.60 dimensionless time units defined by us (366.3 time units owing to the scaling unit adopted by HMW80). The cell of HMW80 would plausibly spread all over the region if the integration were continued.

The experiments of HMW80 corresponding to case FQ do not present a single cell spreading all over the region. As in case FF, the shortage of integration time can be the reason for the difference between the results of HMW80 and ours. Especially in case FQ, if the final wavenumber transition is from wavenumber two to one, the phase change should occur, and hence it takes a longer time for the cells to spread than in case FF. In our experiment case FQ, it takes 50 dimensionless time units before observing the cells with wavenumber one. In the experiment of HMW80 with $Ra = 2.4 \times 10^4$, on the other hand, integration is performed only up to 1.02 dimensionless time units (232.8 time units owing to the scaling unit adopted by HMW80). Their integration time is possibly insufficient for the cells to complete their evolution.

Another possible reason why the convective cell does not evolve to the largest scale in case FQ of HMW80 is the existence of lateral boundaries. Under the lateral boundary conditions adopted by them, the phase change emphasized so far is inhibited by some initial conditions. According to the weak nonlinear theory presented in §4, the position of an upward region must be fixed during the transition of the dominant wavenumber from two to one. A possibility is that, since the existence of a lateral boundary does not allow this condition, the cells cannot spread over the region in HMW80. On the other hand, in the numerical solution of the weak nonlinear theory of CP80, a cell with wavenumber one actually grows in spite of the existence of lateral boundaries. The reason is that the initial condition selected by CP80 has an upward region just at the lateral boundary which satisfies the condition discussed above.

Numerical calculations were performed at the Computer Center of the University of Tokyo, and at the National Institute for Environmental Studies, Environment Agency of Japan. Some of the figures were produced by GFD-DENNOU Library.

Appendix A. Linear theory

In this section, we summarize the results of the linear stability theory of the conductive solutions with no motion for five cases shown in figure 1. The critical Rayleigh number Ra_c and the critical wavenumber k_c under various thermal conditions have been calculated by Rayleigh (1916) for case TT, Jakeman (1968) for case FF, McKenzie, Roberts & Weiss (1974) for case TF and case TQ. In previous studies, the growth rates of unstable modes for $Ra > Ra_c$ have not been presented, except for case TT given by Ogura & Yagihashi (1969). We calculate the growth rates and present the wavenumbers of the most unstable modes for $Ra > Ra_c$.

The temperature distribution of the basic states is

$$T = 1 - z - \tfrac{1}{2}Qz^2, \tag{A 1}$$

where Q is 0 for cases TT, FF and TF, and is -1 for cases FQ and TQ.

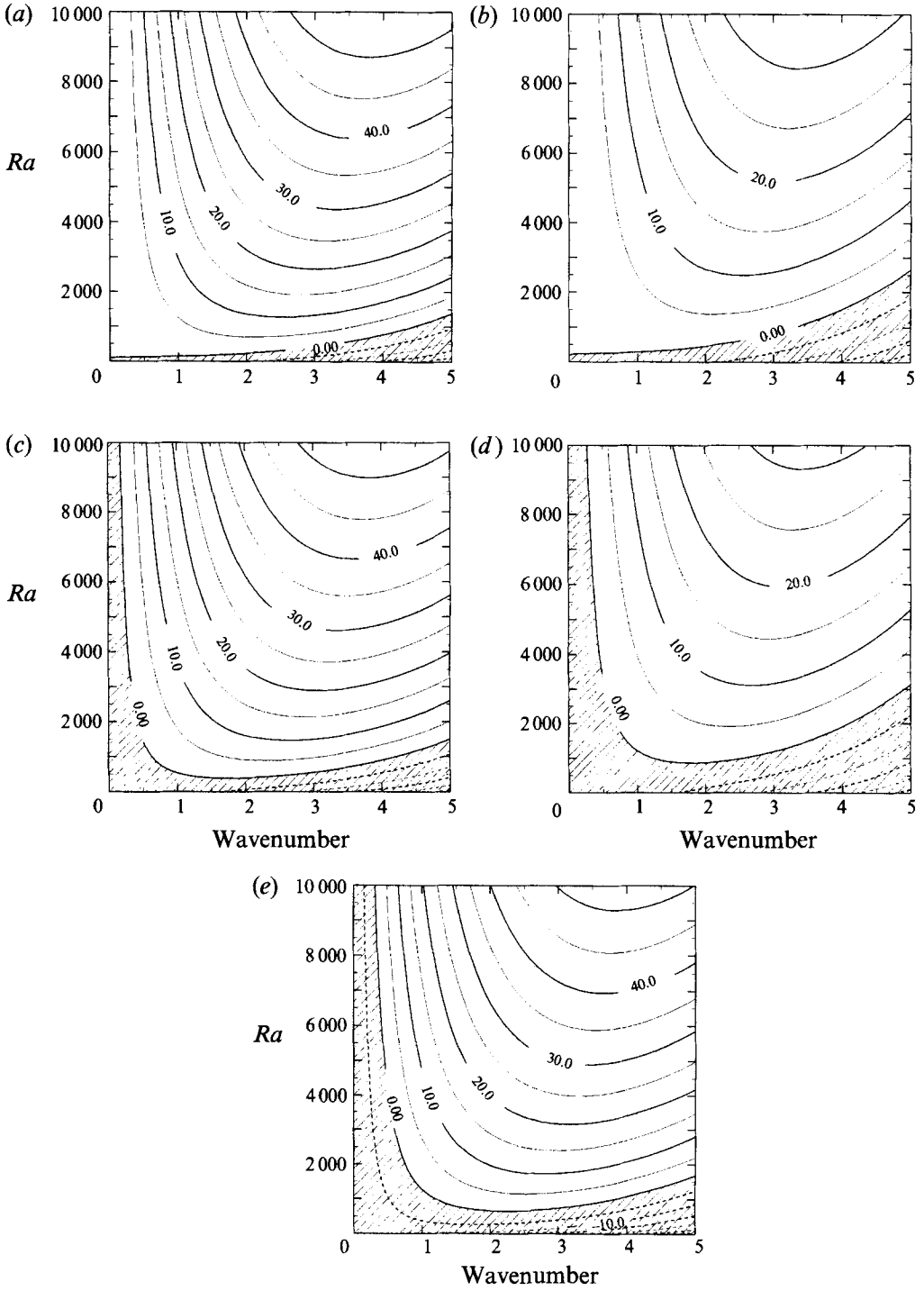

FIGURE 13. The distribution of growth rates of the most unstable modes in (k, Ra) space for $Pr = 1$. (*a*) Case FF, (*b*) case FQ, (*c*) case TF, (*d*) case TQ, (*e*) case TT. The areas of negative values are shaded.

	Case FF	Case FQ	Case TF	Case TQ	Case TT
Ra_c	120.0	240.0	384.7	867.7	654.5
k_c	0.0	0.0	1.76	1.79	2.22

TABLE 2. Critical Rayleigh numbers and critical wavenumbers

	Case FF	Case FQ	Case TF	Case TQ	Case TT
Wavenumber	3.9	3.5	3.9	3.5	3.9

TABLE 3. The wavenumbers of the most unstable modes at $Ra = 10^4$

The equations governing the perturbation, which is expressed by $'$, are

$$\frac{\partial}{\partial t}\nabla^2\frac{\partial \psi'}{\partial x} = Pr\,\nabla^2\nabla^2\frac{\partial \psi'}{\partial x} - Pr\,Ra\frac{\partial^2 T'}{\partial x^2}, \tag{A 2}$$

$$\frac{\partial T'}{\partial t} = -(1+Qz)\frac{\partial \psi'}{\partial x} + \nabla^2 T'. \tag{A 3}$$

Figure 13 shows the distribution of the growth rates in (k, Ra) space. These figures are given numerically with twenty vertical grid points. In case FF (figure 13*a*) and case FQ (figure 13*b*), the critical wavelength becomes infinite. However, at $Ra \gtrsim 1000$, the wavenumber of the most unstable modes are from two to four regardless of the thermal conditions.

The values of the critical Rayleigh numbers and the critical wavenumbers for five cases are shown in table 2. The values of the wavenumber of the most unstable modes at $Ra = 10^4$ which is the value adopted in our numerical integrations are shown in table 3.

Appendix B. The derivation of equation (9)

We summarize the derivation of the equation given by CP80, which governs the leading-order evolution of temperature in cases FF and FQ. Let us assume the Rayleigh number to be expressed as $Ra = Ra_c + \mu^2\epsilon^2$ ($\epsilon \ll 1, \mu = O(1)$). We rescale time and horizontal length as $\epsilon^4 t \to t$, $\epsilon x \to x$ and expand temperature and stream function in powers of ϵ as

$$T = \theta_0 + \epsilon^2\theta_2 + \ldots, \tag{B 1}$$

$$\psi = \epsilon\phi_0 + \epsilon^3\phi_2 + \ldots . \tag{B 2}$$

Substituting (B 1) and (B 2) into (3) and (4), we obtain, from the $O(\epsilon^0)$ equation of temperature

$$0 = \frac{\partial^2\theta_0}{\partial z^2}, \tag{B 3}$$

which means that θ_0 does not depend on z. From the $O(\epsilon^0)$ equation of vorticity, we have

$$0 = \frac{\partial^4\phi_0}{\partial z^4} - Ra_c\frac{\partial\theta_0}{\partial x}. \tag{B 4}$$

The $O(\epsilon^2)$ equations are

$$\frac{1}{Pr}\left\{-\frac{\partial\phi_0}{\partial x}\frac{\partial^3\phi_0}{\partial z^3}+\frac{\partial\phi_0}{\partial z}\frac{\partial^3\phi}{\partial x\partial z^2}\right\}=2\frac{\partial^4\phi_0}{\partial x^2\partial z^2}+\frac{\partial^4\phi_2}{\partial z^4}-Ra_c\frac{\partial\theta_2}{\partial x}-\mu^2\frac{\partial\theta_0}{\partial x}, \tag{B 5}$$

$$-\frac{\partial\phi_0}{\partial x}\frac{\partial\theta_0}{\partial z}+\frac{\partial\phi_0}{\partial z}\frac{\partial\theta_0}{\partial x}=-\frac{\partial\phi_0}{\partial x}(1+Qz)+\frac{\partial^2\theta_0}{\partial x^2}+\frac{\partial^2\theta_2}{\partial z^2}, \tag{B 6}$$

and the $O(\epsilon^4)$ equation of temperature is

$$\frac{\partial\theta_0}{\partial t}-\frac{\partial\phi_0}{\partial x}\frac{\partial\theta_2}{\partial z}-\frac{\partial\phi_2}{\partial x}\frac{\partial\theta_0}{\partial z}+\frac{\partial\phi_0}{\partial z}\frac{\partial\theta_2}{\partial x}+\frac{\partial\phi_2}{\partial z}\frac{\partial\theta_0}{\partial x}=-\frac{\partial\phi_2}{\partial x}(1+Qz)+\frac{\partial^2\theta_2}{\partial x^2}+\frac{\partial^2\theta_4}{\partial z^2}. \tag{B 7}$$

The equation for $\theta_0(x,t)$ can be obtained by integrating (B 4) $\sim$ (B 7) with z and eliminating ϕ_0, ϕ_2, θ_2:

$$\frac{\partial\theta_0}{\partial t}=-A\mu^2\frac{\partial^2\theta_0}{\partial x^2}-B\frac{\partial^4\theta_0}{\partial x^4}+C\frac{\partial}{\partial x}\left\{\left(\frac{\partial\theta_0}{\partial x}\right)^3\right\}-D\frac{\partial}{\partial x}\left(\frac{\partial\theta_0}{\partial x}\frac{\partial^2\theta_0}{\partial x^2}\right). \tag{B 8}$$

The coefficients $A \sim D$ are defined as follows.

$$A\equiv\int_0^1 P(z)(Qz+1)\,dz=\frac{1}{Ra_c}, \tag{B 9}$$

$$\begin{aligned}B\equiv{}&2Ra_c\int_0^1\{P'(z)\}^2\,dz-\int_0^1\left[\int_0^{z_2}\{Ra_c P(z_1)(1+Qz_1)-1\}\,dz_1\right]^2 dz_2\\&-\int_0^1 Ra_c P(z_3)\,Qz_3\int_0^{z_3}\int_0^{z_2}\{Ra_c P(z_1)(1+Qz_1)-1\}\,dz_1\,dz_2\,dz_3\\&-Q\int_0^1 2R_c N(z)\,P''(z)\,dz+Q\int_0^1 N(z)\,Ra_c\int_0^{z_3}\int_0^{z_2}\{R_c P(1+Qz_1)-1\}\,dz_1\,dz_2\,dz_3,\end{aligned} \tag{B 10}$$

$$C\equiv\int_0^1 Ra_c^2\{P(z)\}^2\,dz, \tag{B 11}$$

$$\begin{aligned}D\equiv{}&-\frac{3}{2}\frac{Ra_c^2}{Pr}\int_0^1\{P'(z)\}^3\,dz+Q\frac{R_c^2}{Pr}\int_0^1 N(z)\{-P(z)\,P'''(z)+P'(z)\,P''(z)\}\,dz\\&+Q\int_0^1 2R_c^2 N(z_2)\int_0^{z_2}P(z_1)\,dz_1\,dz_2-3\int_0^1 Ra_c P(z_2)\int_0^{z_2}\{Ra_c P(z_1)(1+Qz_1)-1\}\,dz_1\,dz_2\\&-2\int_0^1 Ra_c P(z_2)\,Qz_2\int_0^{z_2}R_c P(z_1)\,dz_1\,dz_2,\end{aligned} \tag{B 12}$$

where $P(z), N(z)$ are polynomials given by

$$P(z)\equiv\tfrac{1}{24}z^4-\tfrac{1}{12}z^3+\tfrac{1}{24}z, \tag{B 13}$$

$$N(z)\equiv\tfrac{1}{120}z^5-\tfrac{1}{36}z^3+\tfrac{7}{360}z. \tag{B 14}$$

By evaluating each term in (B 12), it can be shown that $D=0$ if $Q=0$. The dependency on Pr appears only in (B 12). When $Pr=1$, we have, for case FF,

$$A=\tfrac{1}{120},\quad B=\tfrac{1091}{5544},\quad C=\tfrac{155}{126},\quad D=0, \tag{B 15}$$

and for case FQ,

$$A=\tfrac{1}{240},\quad B=\tfrac{15866}{81081},\quad C=\tfrac{310}{63},\quad D=-\tfrac{613}{2079}. \tag{B 16}$$

By replacing $(A/B)^{1/2}x \to x$, $A^2/Bt \to t$, $(C/B)^{1/2}\theta_0 \to \theta_0$ and $\alpha \equiv D/(BC)^{1/2}$, (B 8) is translated into (9).

REFERENCES

BJERKNES, J. 1938 Saturated-adiabatic ascent of air through dry-adiabatically descending environment. *Q. J. R. Met. Soc.* **64**, 325–330.

BUSSE, F. H. & WHITEHEAD, J. A. 1971 Instability of convection rolls in a high Prandtl number fluid. *J. Fluid Mech.* **51**, 305–320.

CHAPMAN, C. J., CHILDRESS, S. & PROCTOR, M. R. E. 1980 Long wavelength thermal convection between non-conducting boundaries. *Earth Planet. Sci. Lett.* **51**, 362–369 (referred to herein as CCP80).

CHAPMAN, C. J. & PROCTOR, M. R. E. 1980 Nonlinear Rayleigh–Bénard convection between poorly conducting boundaries. *J. Fluid Mech.* **101**, 759–782 (referred to herein as CP80).

HEWITT, J. M., MCKENZIE, D. P. & WEISS, N. O. 1980 Large aspect ratio cells in two-dimensional thermal convection. *Earth Planet. Sci. Lett.* **51**, 370–380 (referred to herein as HMW80).

HURLE, D. T. J., JAKEMAN, E. & PIKE, E. R. 1967 On the solution of the Bénard problem with boundaries of finite conductivity. *Proc. R. Soc. Lond.* A **296**, 469–475.

JAKEMAN, E. 1968 Convective instability in fluids of high thermal diffusivity. *Phys. Fluids* **11**, 10–14.

MCKENZIE, D. P., ROBERTS, J. M. & WEISS, N. O. 1974 Convection in the earth's mantle: towards a numerical simulation. *J. Fluid Mech.* **62**, 465–538.

MADDEN, R. A. & JULIAN, P. R. 1972 Description of global-scale circulation cells in the tropics with 40–50 day period. *J. Atmos. Sci.* **29**, 1109–1123.

NUMAGUTI, A. & HAYASHI, Y.-Y. 1991*a* Behaviors of cumulus activity and the structures of circulations in an 'aqua planet' model. Part I: The structure of the super clusters. *J. Met. Soc. Japan* **69**, 541–561.

NUMAGUTI, A. & HAYASHI, Y.-Y. 1991*b* Behaviors of cumulus activity and the structures of circulations in an 'aqua planet' model. Part II: Eastward moving planetary scale structure and the intertropical convergence zone. *J. Met. Soc. Japan* **69**, 563–579.

OGURA, Y. 1971 A numerical study of wavenumber selection in finite-amplitude Rayleigh convection. *J. Atmos. Sci.* **28**, 709–717.

OGURA, Y. & YAGIHASHI, A. 1969 A numerical study of convection rolls in a flow between horizontal parallel plates. *J. Met. Soc. Japan* **47**, 205–217.

RAYLEIGH, LORD 1916 On convection currents in a horizontal layer of fluid, when the higher temperature is on the under side. *Phil. Mag.* **32**, 529–546.

ROTHERMEL, J. & AGEE, E. M. 1986 A numerical study of atmospheric convective scaling. *J. Atmos. Sci.* **43**, 1185–1197.

SASAKI, Y. 1970 Influences of thermal boundary layer on atmospheric cellular convection. *J. Met. Soc. Japan* **48**, 492–502.

SCHLÜTER, A., LORTZ, D. & BUSSE, F. 1965 On the stability of steady finite amplitude convection. *J. Fluid Mech.* **23**, 129–144.

SPARROW, E. M., GOLDSTEIN, R. J. & JONSSON, V. K. 1964 Thermal instability in a horizontal fluid layer: effect of boundary conditions and nonlinear temperature profile. *J. Fluid Mech.* **18**, 513–528.

SYKES, R. I. & HENN, D. S. 1988 A note on the numerical computation of two-dimensional convective flow. *J. Atmos. Sci.* **45**, 1961–1964.

XIE, S.-P. 1994 On preferred zonal scale of wave-CISK with conditional heating. *J. Met. Soc. Japan* **72**, 19–30.